Iranian Journal of Oil & Gas Science and Technology, Vol. 9 (2020), No. 1, pp. 68-84
http://ijogst.put.ac.ir

Effect of Surface Roughness on Vortex Length and Efficiency of Gas-oil Cyclones through CFD Modelling

Seyed Masoud Vahedi[1], Farzad Parvaz[2*], Mohsen Khandan Bakavoli[1], and Mohammad Kamali[3]

[1] M.S. Student, Department of Mechanical Engineering, Semnan University, Semnan, Iran
[2] PhD. Candidate, Department of Mechanical Engineering, Najafabad Branch, Islamic Azad University, Isfahan, Iran
[3] M.S. Student, Department of Mechanical Engineering, Najafabad Branch, Islamic Azad University, Isfahan, Iran

Received: October 27, 2017; *revised*: December 01, 2017; *accepted*: January 08, 2017

Abstract

Separation of suspended droplets in a fluid flow has been a great concern for scientists and technologists. In the current study, the effect of the surface roughness on flow field and the performance of a gas-oil cyclone is studied numerically. The droplets and the turbulent airflow inside the cyclone are considered to be the discrete and continuous phases respectively. The Reynolds stress model (RSM) is employed to simulate the complex, yet strongly anisotropic, flow inside the cyclone while the Eulerian-Lagrangian approach is selected to track droplet motion. The results are compared to experimental studies; according to the results, the tangential and axial velocities, pressure drop, and Euler number decrease when the surface roughness increases. Moreover, the cyclone efficiency drops when the vortex length decreases as a result of a rise in surface roughness. The differences between the numerical and experimental results become significant at higher flow rates. By calculating the impact energy of droplets and imposing the film-wall condition on the walls, splash does not occur.

Keywords: Roughness, Reynolds Stress Tensor, Eulerian-Lagrangian, Oil-gas Cyclone, Two-phase flow

1. Introduction

An aerocyclone is a device to which a gas-oil mixture is introduced from the inlet channel(s) located near the upper section, and the separation happens in the lower part (Brar et al., 2015). The separation happens as a result of the centrifugal and gravitational forces. Due to their simplicity and ease of installation, aerocyclones are used in a wide range of applications in gas and petroleum industries. The prediction of cyclone performance relies on a good understanding of flow behavior and geometric parameters which influence the flow pattern (Elsayed and Lacor, 2011).

Many researchers have estimated the cyclone efficiency by presenting various mathematical models which are based on physical phenomena happening inside the cyclone (Brar et al., 2015; Baltrenas

* Corresponding author:
Email: f.parvaz@semnan.ac.ir

and Chlebnikovas, 2015). Some neglect the surface friction in their numerical investigations of cyclone aerodynamics (Shukla et al., 2013; Xianget al., 2001; Hosseini et al., 2015). The surface friction of a cyclone depends on roughness characteristics due to corrosion and/or collision and the accumulation of particles on the surface. Therefore, the surface roughness is an important parameter remarkably affecting the cyclone performance. The friction factor was first presented by Barth (1956) who calculated the tangential velocity of the gas in the vortex flow. He also evaluated the pressure drop and the cyclone performance for the Rankine vortex region. The relation extracted by Barth for pressure drop consisted of the wall and outlet loss terms. Barth's model was extended by Muschelknautz and Krambrock (1970) when they modified the friction coefficient and investigated the friction impact by injecting and adding solid materials to cyclone walls; their model estimated the efficiency more accurately. Meissner and Loffler (1978) derived an empirical expression for the tangential velocity which took the wall friction into account. This model also included two additional friction factors. Karagoz and Avci (2005) presented another model to predict the pressure drop and the efficiency of the cyclone. Unlike other studies, their friction coefficient was a function of the Reynolds number and the surface roughness. They showed that the wall friction reduces the vortex flow, and as a consequence, the pressure drop decreases, which was considered to be constant in all models. Zhou et al. (2017) studied the effect of roughness on the vortex length and the efficiency of gas-particle cyclones. Their results showed that some particles cause surface abrasion, and as a result, they significantly increase surface roughness. Also, they reported that the appropriate cyclone surface roughness should be controlled to obtain the optimal separation performance for an optimized cyclone separator. Kaya et al. (2011) investigated the flow field and efficiency of two types of cyclone using commercial CFD software. There was good agreement between their numerical simulation results and experimental data. Wang et al. (2006) studied the impacts of particle size and gas inlet velocity on the performance and gas flow field of the Lapple cyclone. They indicated that an increase in particle size and volumetric gas flow rate raises the cyclone performance. A particle-laden flow was simulated in three different cyclones by Shi and Bayless (2007). They verified their results by comparing them with the experimental data. Raoufi et al. (2008) and Kępa (2010) studied the flow field inside the cyclones with different outlet geometries and concluded that these geometries significantly affect the performance of the aerocyclones.

In the present study, a comprehensive research is conducted to evaluate the effects of roughness, inlet velocity, and droplet diameter on the efficiency of a Stairmand cyclone. The dimensionless distribution of tangential and axial velocities are illustrated for three different materials with three distinct roughness values. The performance of the cyclone was studied at various droplet sizes in a gas-droplet mixture. The RSM model was utilized to simulate the turbulent flow, whereas the Eulerian-Lagrangian statistical approach was employed to investigate the cyclone performance. The length of vortex flow, which is an essential factor in the separation of water droplets, is also calculated. Further, the probability of splashing is considered.

2. Conceptual model

The Stairmand cyclone consists of four parts, namely inlet channel, central cylinder, vortex finder, and the cone section (see Figure 1). The dimensions of these parts are listed in Table 1. The two-phase flow of fluid and water droplet are blown through the cyclone inlet channel tangentially. The tangential velocity decreases when the current moves down the cyclone until it reaches the cone section where the decreasing trend of tangential velocity is inverted. In the cone section, where the second vortex formation happens, lighter water droplets are moved by the centrifugal force originated from tangential velocity towards the flow core, and they ascended to the cyclone outlet.

Table 1

Geometrical properties of the cyclone investigated in the present work.

Parameters	D	a	b	D_x	S	B_c	h	H_t	L_e	L_i
Dimensional (m)	0.290	0.145	0.058	0.145	0.145	0.108	0.435	0.1160	0.435	0.290
Nondimensional	1	0.5	0.2	0.5	0.5	0.375	1.5	4	1.5	1

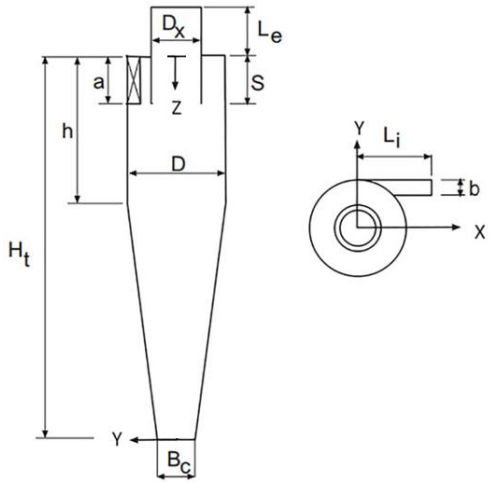

Figure 1

A schematic representation of Stairmand cyclone geometry.

3. Governing equations

3.1. Continuous phase

The fluid flow inside a cyclone is three-dimensional, turbulent, and isothermal. Since the maximum fluid velocity in the cyclone is 20 ms^{-1} at the inlet, the Mach number is equal to 0.06; therefore, the flow can be considered incompressible. The Reynolds averaged Navier-Stokes and continuity equations can be written as follows (Parvaz et al., 2017; Gao et al., 2013);

$$\frac{\partial \overline{u_i}}{\partial x_i} = 0 \tag{1}$$

$$\frac{\partial \overline{u_i}}{\partial t} + \overline{u_j}\frac{\partial \overline{u_i}}{\partial x_j} = -\frac{1}{\rho}\frac{\partial \bar{p}}{\partial x_i} + \nu\frac{\partial^2 \overline{u_i}}{\partial x_j \partial x_j} - \frac{\partial}{\partial x_j}R_{ij} \tag{2}$$

3.2. Turbulence modeling

Since the flow inside the cyclone is a high-speed swirling flow, the RSM model is applied. Streamlines with high curvatures, swirl, rotation, and rapid changes in the strain rate could be simulated in a more rigorous manner with RSM than with one-equation and two-equation turbulent models (Parvaz et al., 2017; ANSYS Fluent User's Guide 2013; Sun et al., 2017). Thus, the following relations can be used:

$$\frac{\partial}{\partial t}\left(\rho\overline{\acute{u}_i\acute{u}_j}\right) + \overline{u_k}\frac{\partial}{\partial x_k}\left(\rho\overline{\acute{u}_i\acute{u}_j}\right) = D_{T,ij} + P_{ij} + \theta_{ij} - \varepsilon_{ij} \tag{3}$$

The first term on the right-hand side of the above equation represents turbulent diffusion term which is expressed by:

$$D_{T,ij} = \frac{\partial}{\partial x_k}\left(\frac{\mu}{\sigma^k}\frac{\partial \overline{\acute{u}_i \acute{u}_j}}{\partial x_k}\right) \tag{4}$$

The second term refers to stress production term:

$$P_{ij} = -\rho\left(\overline{\acute{u}_i \acute{u}_k}\frac{\partial \overline{u}_j}{\partial x_k} + \overline{\acute{u}_j \acute{u}_k}\frac{\partial \overline{u}_i}{\partial x_k}\right) \tag{5}$$

The third term is also known as the pressure-strain correlation term:

$$\theta_{ij} = p\overline{\left(\frac{\partial \acute{u}_i}{\partial x_j} + \frac{\partial \acute{u}_j}{\partial x_i}\right)} \tag{6}$$

The last term is called the dissipation term:

$$\varepsilon_{ij} = 2\mu\overline{\frac{\partial \acute{u}_i}{\partial x_k}\frac{\partial \acute{u}_j}{\partial x_k}} \tag{7}$$

3.3. Discrete phase

The effect of droplets on the change in flow field can be neglected when the assumption of the low volume fraction (less than 10%) is considered for the droplets. The governing equation for droplet motion is given as follows:

$$\frac{d\overrightarrow{u_d}}{dt} = F_D(\vec{u} - \overrightarrow{u_d}) + \vec{\mathrm{g}}\frac{(\rho_d - \rho)}{\rho_d} + \overrightarrow{F_i} \tag{8}$$

where, $\overrightarrow{u_d}$ is droplet velocity, and $F_D(\vec{u} - \overrightarrow{u_d})$ stands for the drag force imposed to droplets. ρ_p, g, and $\overrightarrow{F_i}$ represent droplet density, gravitational acceleration, and other forces like Brownian and Soffman's lift forces respectively (Kaya et al., 2011). In the current study, these two latter forces are not considered. For spherical droplets, the drag force can be written by:

$$F_D = \frac{18\mu}{\rho_d d_d^2}\frac{C_D Re_p}{24} \tag{9}$$

where, the Reynolds number is calculated by (Parvaz et al., 2017):

$$Re_d = \frac{\rho_d d_d |\vec{u} - \overrightarrow{u_d}|}{\mu} \tag{10}$$

Four regimes of droplet behavior, namely stick, rebound, spread, and splash regimes, could happen for droplets while the chance of occurrence depends on the impact energy and the cyclone wall temperature (see Figure 2).

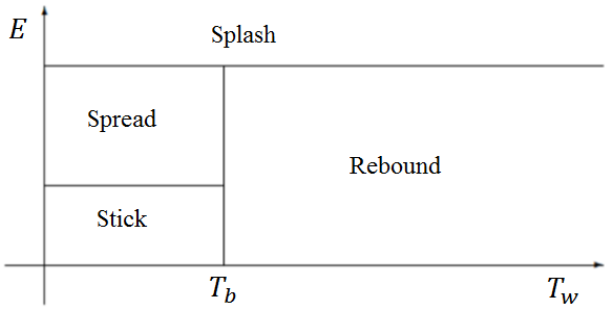

Figure 2

Four regimes of droplet behavior (ANSYS Fluent User's Guide 2013).

Splashing has been studied in the current work at a constant wall temperature of 273 K. Below the boiling temperature of the liquid, the droplets can either stick, spread, or splash, whereas above the boiling temperature, the droplets can either rebound or splash. It should be noted again that the occurrence of these regimes depends on the impact energy and boiling temperature of the liquid. The dimensionless impact energy of the droplets can be defined as:

$$E^2 = \frac{\rho V_r^2 D}{\sigma}\left(\frac{1}{min\left(\frac{h_0}{D},1\right)+\frac{D}{Re\sqrt{Re}}}\right) \tag{11}$$

When E becomes less than 16, the sticking regime is applied, which means that the velocity of the droplet is the same as the wall velocity. Nevertheless, at wall temperatures higher than the boiling temperature of liquid, the impact energy is less than the critical energy. Splashing happens when the impact energy is higher than a critical energy threshold 57.7 (ANSYS Fluent User's Guide 2013).

3.4. Wall roughness

The flow resistance, specifically because of surface roughness, causes momentum transport, especially in the boundary layer. Hence, the law of the wall is influenced by the surface roughness, and it can be modified as follows:

$$\frac{\bar{u}}{u_\tau} = \frac{1}{\kappa}\ln\left(\frac{yu_\tau}{\nu}\right) + B - \Delta B(k_s^+) \tag{12}$$

where, κ (Von-Karman constant) equals 0.41, and B is an empirical constant for smooth walls set at 5.56 (Sun et al., 2017).

For the hydraulically rough flows, the roughness function is expressed in:

$$\Delta B = \frac{1}{\kappa}\ln\left(\frac{k_s^+ - 2.25}{87.75} + c_s k_s^+\right) \times \sin[0.4258\ln(k_s^+ - 0.811)] \tag{13}$$

where, c_s is a constant equal to 0.5 (Sun et al., 2017).

3.5. Vortex length

The outer vortex flow axis changes when its distance from the vortex finder increases. This downward vortex flow is known as the free vortex flow as schematically demonstrated in Figure 3. The free

vortex length is calculated using the radial distribution of pressure inside the cyclone. This parameter is rarely considered to investigate the droplets efficiency; however, it has a vital role in cyclone performance estimation (Alahmadi and Nowakowski, 2016; Alexander, 1949; Bryant et al., 1983; Ji et al., 1991).

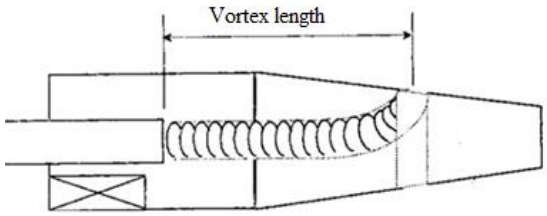

Figure 3

The free vortex length of a cyclone.

Although the vortex length is almost unpredictable, a number of correlations are presented for it. Alexander (1949) presented a relation for the free vortex length of a glassy cyclone (30.2 to 200 mm).

$$\frac{L}{D} = 2.3\frac{D_x}{D}\left(\frac{D^2}{ab}\right)^{\frac{1}{3}} \tag{14}$$

Bryant et al. (1983) and Ji et al. (1991) also reported empirical Equations 15 and 16 respectively:

$$\frac{L}{D} = 2.26\left(\frac{D_x}{D}\right)^{-1}\left(\frac{D^2}{ab}\right)^{-0.5} \tag{15}$$

$$\frac{L}{D} = 2.4\left(\frac{D_x}{D}\right)^{-2.25}\left(\frac{D^2}{ab}\right)^{-0.361} \tag{16}$$

3.6. Boundary conditions

After preparing the geometry and grids, the boundary conditions should be specified (Sabziani and Sari, 2015). The air flow enters the cyclones tangentially at a velocity of $10\ \mathrm{ms}^{-1}$. The air flow exits from the cyclone through the vortex finder mounted on top of the cyclone. No-slip boundary condition is considered for all the walls. The bottom section is regarded as a trap to study the cyclone performance (Parvaz et al., 2017). The wall-film model is applied to the walls so as to investigate the splashing. The wall roughness of the three different materials used in producing the cyclone is listed in Table 2.

Table 2

The surface roughness of the substances used in the cyclone (Shames, 1982).

Material	Glass	Steel (wrought iron)	Galvanized iron
Roughness (mm)	0.0003	0.046	0.15

4. Solver settings

The detailed information used in the present CFD modeling such as the discretization scheme of pressure, momentum, turbulent kinetic energy, turbulent dissipation rate, the Reynolds stress, and pressure/velocity coupling are tabulated in Table 3.

Table 3

Numerical setting of the current simulation.

Numerical setting	Pressure discretization	Pressure velocity coupling	Momentum discretization	Turbulent kinetic energy	Turbulent dissipation rate	Reynolds stress
Scheme	Body force weighted	SIMPLE	QUICK	Second-order upwind	Second-order upwind	First-order upwind

According to the related literature, the turbulence intensity and turbulence characteristic length are set at 5% and 0.07 times of the inlet width respectively. The discrete phase loading was considered to be 0.005 kg per the unit volume of air with a mean diameter of 6.76 μm and a geometric standard deviation of 2.08. Using Rosin-Rammler distribution function, the relationship between droplet diameter and the mass fraction of droplets can be obtained (Fathizadeh et al., 2015).

$$R(d) = \exp\left[-\left(d/\bar{d}\right)^{n}\right] \tag{17}$$

where, $\bar{d}$ and n represent the characteristic diameter and distribution parameter respectively. The size of the droplets is selected in the range of 0.1 to 14 μm. The droplets are injected in the face normal condition at a velocity equal to that of the flowing fluid at the cyclone inlet, and discrete phase model (DPM) setting is defined as a trap at the bottom of the cyclone. The droplets reach the cyclone walls, collide with them, and reflect off them. Under the low droplet loading condition, it is entirely reasonable to assume that the collision of discrete phase droplets with the cyclone walls is perfectly elastic; hence, the coefficients of restitution (COR) in tangential as well as normal directions of the walls are considered to be unity (Fathizadeh et al., 2015).

The residence time of an unsteady simulation is obtained by the following relation (Parvaz et al., 2017):

$$t_{res} = \frac{\forall}{Q} \tag{18}$$

The calculated residence time of the present simulation is equal to 0.73 s.

5. Grid independence study

Hexagonal cells produced via Gambit software are depicted in Figure 4. To prevent variations in the results with grid size, the static pressure drop was used as a criterion to study the mesh independency. Several grids were generated as listed in Table 4. In addition to pressure, the results of studying grid independence are demonstrated for tangential and axial velocities at Z=0.75D in Figure 5. According to Table 3 and the profile of velocities, a geometry containing 765520 cells with an error of 0.96% was selected.

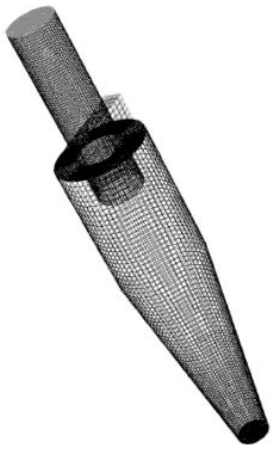

Figure 4

Grid generation.

Table 4

Details of grid independence study.

Number of cells	585424	630952	765520
Static pressure drop (□□)	339.487	355.104	358.522
Deviation (%)	-	4.6	0.96

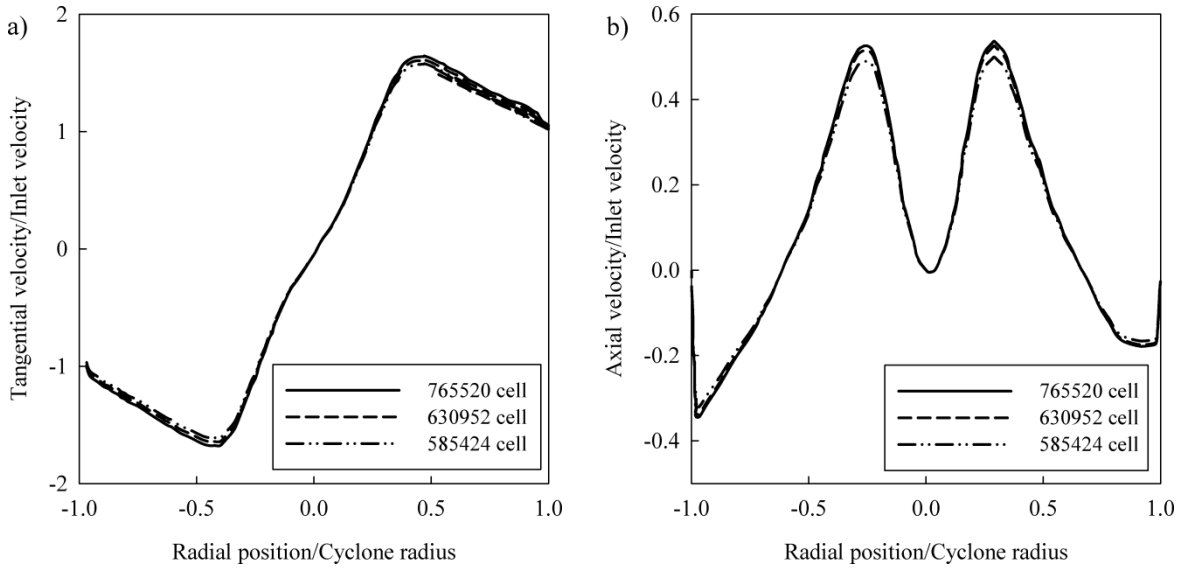

Figure 5

Grid independence study of a) the tangential velocity and b) the axial velocity.

The validity range of the logarithmic-law for mean velocity is 11.225 < y+ < 300, while the laminar stress-strain relationship is valid for y+ < 11.225. The distance of the first grid center from the wall was checked to lie within the range of the logarithmic-law (11.225 <y+ < 300), which is the default range in FLEUNT (see Figure 6).

By comparing the obtained results with the experimental data of Hoekstra (2000), the present study is validated. The comparison between the numerical results and experimental data on the axial and

tangential velocities and pressure drop is displayed in Figures 7 and 8a. Moreover, the results of the dispersed phase are compared to the experimental data of Ehteram et al. (2012) as shown in Figure 8b. It can be seen that the present study simulates the continuous and discrete phases inside the cyclone at an acceptable degree of accuracy.

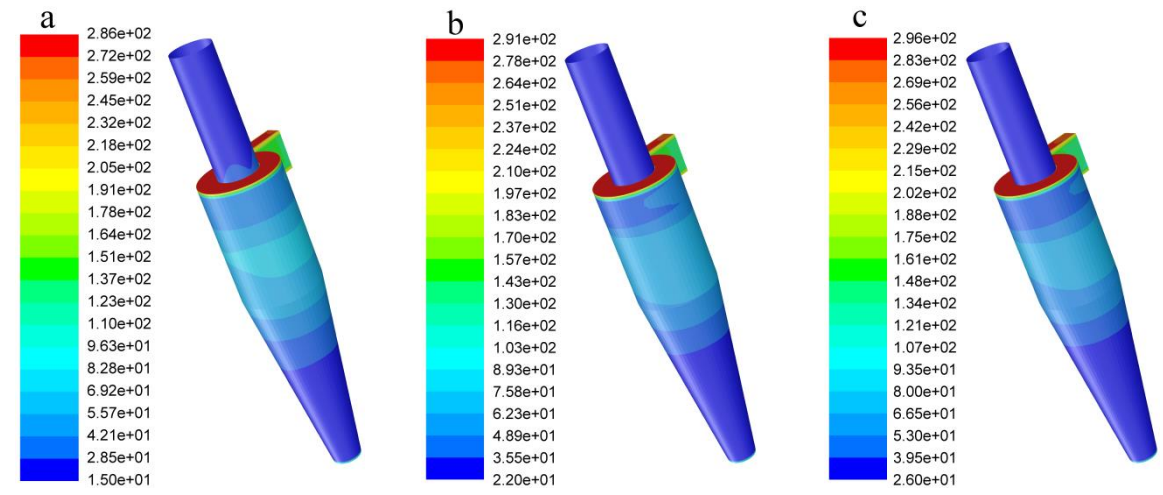

Glass Steel (wrought iron) Galvanized iron

Figure 6

Contour plots of the wall y+ for a) glass, b) steel (wrought iron), and c) galvanized iron.

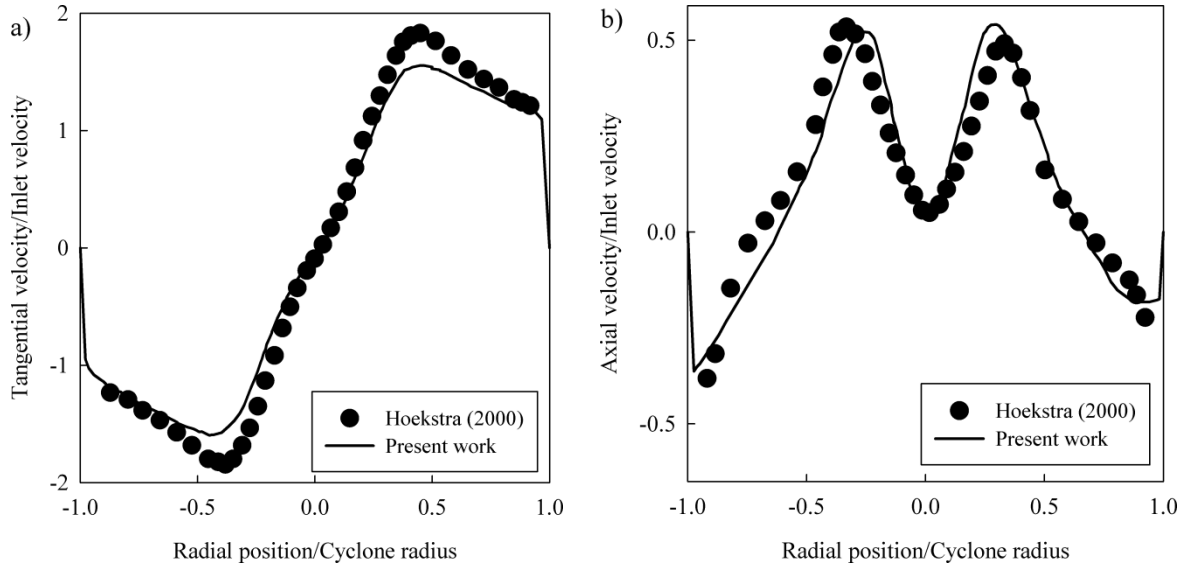

Figure 7

The comparison of the profiles of a) tangential velocity and b) axial velocity between the current numerical simulation and the experimental data of Hoekstra (2000) in the section Z = 0.75D.

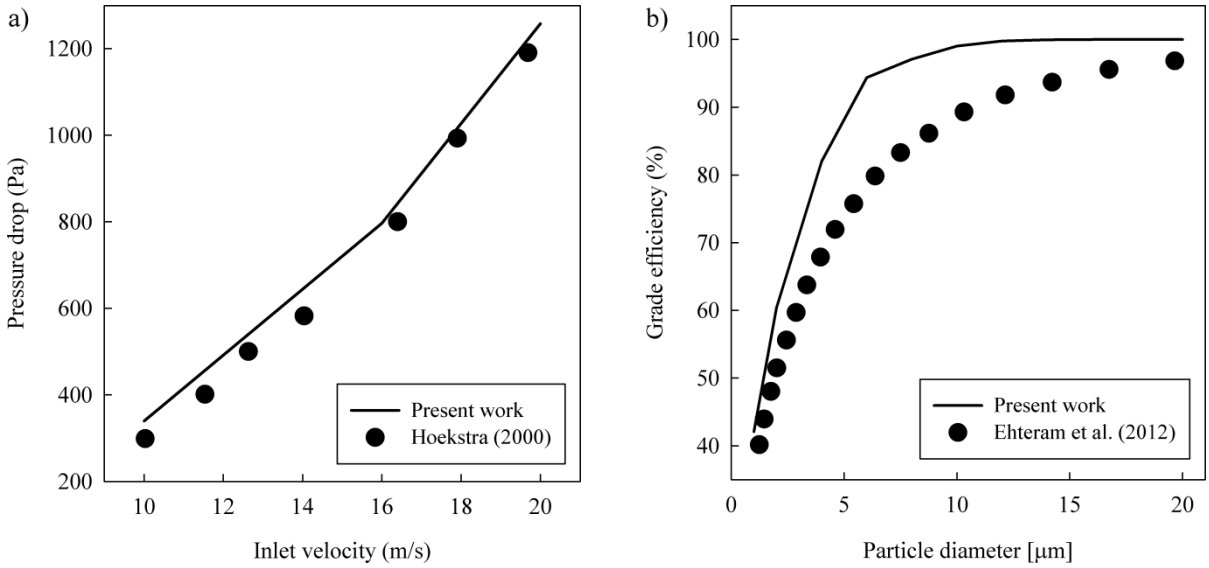

Figure 8

The comparison of the numerical simulation data on a) pressure drop and b) grade efficiency respectively with the works of Hoekstra (2000) and Ehteram et al. (2012).

6. Results and discussion

6.1. Tangential velocity distribution

The tangential velocity has an S-shaped profile as can be seen in Figure 7a. It is divided into two parts. The first part is a forced vortex flow which is mainly located in the central region of the cyclone, and the second part is a free vortex region far from the central axis of the cyclone. In this region, the dissipation increases while the velocity declines. The sum of these two areas is known as Rankine vortex. The effect of roughness on tangential velocity distribution is depicted in Figure 9. As it is obvious, an increase in velocity results in a rise in pressure, which is originated from the swirling flow of gas and its contraction at the entrance of the outlet tube. According to the tangential velocity distributions in Figure 9, the tangential velocity forms both of the regions. Adding roughness to the cyclone walls leads to a rise in the friction between the gas flow and the wall, which reduces the radial distribution of tangential velocity. Therefore, the velocity distribution of glass is located at a higher level than the distributions of steel (wrought iron) and galvanized iron. Although roughness has no noticeable effect on the radial distribution of tangential velocity, its influence on the erosion rate is really important in industry. It is worth noting that increasing roughness shrinks the Rankine vortex region and subsequently reduces the cyclone performance.

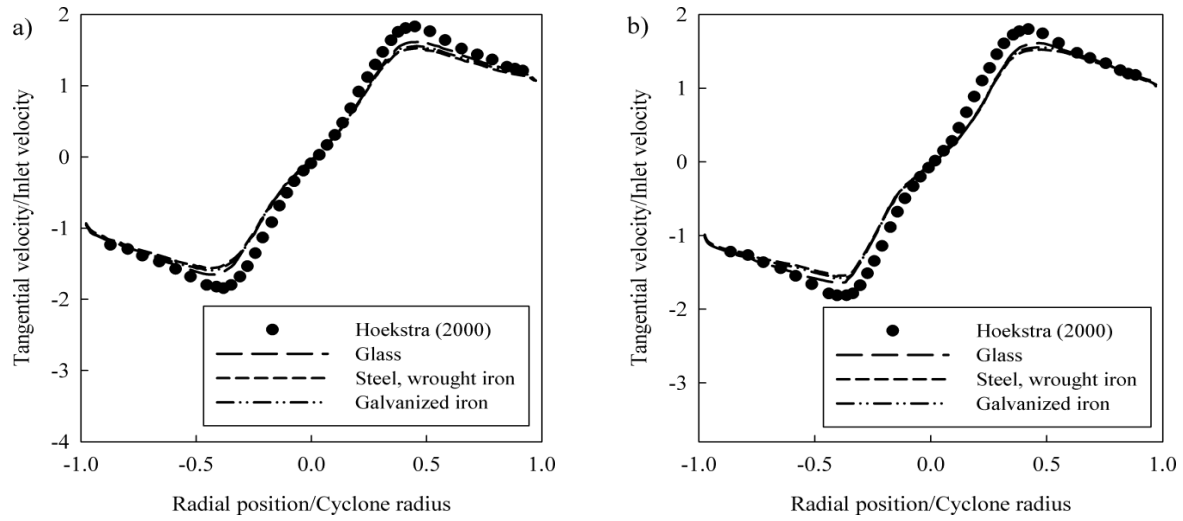

Figure 9

Radial distribution of tangential velocity by considering the wall roughness: a) Z = 0.75D and b) Z = 0.625D.

6.2. Axial velocity distribution

The axial velocity has an essential role in the separation of droplets. According to Figure 7b and experimental data, the axial velocity profile is M-shaped, and an outer vortex flow is created due to descending gas flow. Following that, the inner vortex flow is formed after the first vortex flow impacts on the bottom of the cyclone, which transfers small droplets through the vortex finder.

Axial velocity influences both the flow pattern and cyclone performance. The axial velocity distributions at different roughness values are illustrated in Figure 10 at Z = 0.75D and Z = 0.625D. The gas flow has a downward trend near the walls, while it experiences an upward trend in the central part of the cyclone. This phenomenon is known as a reverse flow. Since the outer downward flow rises with an increase in radius, but the upward inner flow increases by a decrease in radius, the maximum axial velocity happens at the central axis of the cyclone. Therefore, the wall roughness has a more significant effect on the upward flow than the downward flow.

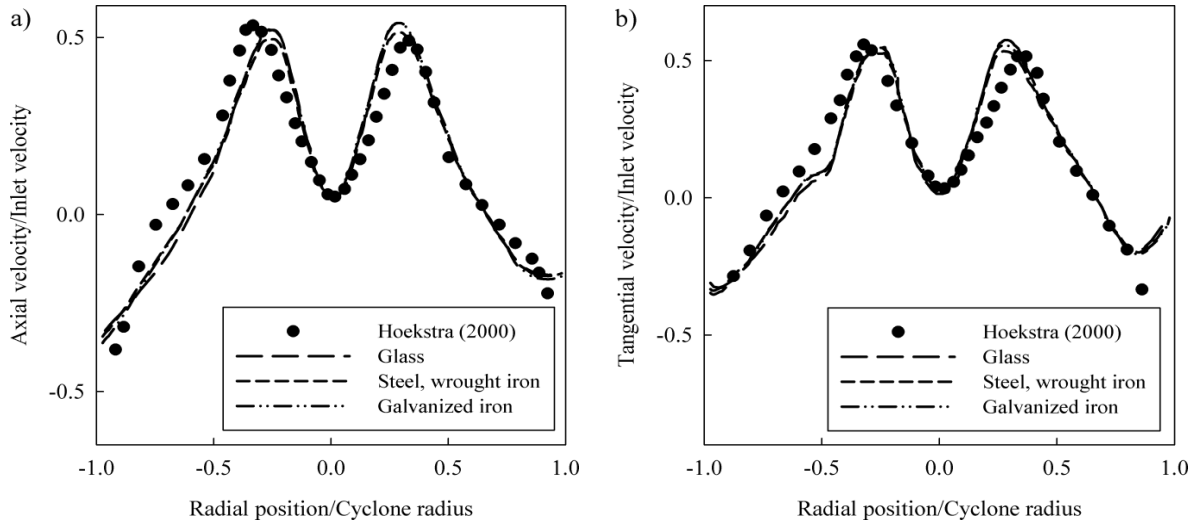

Figure 10

Radial distribution of axial velocity by considering the wall roughness: a) Z = 0.75D and b) Z = 0.625D.

6.3. Pressure distribution

The impact of surface roughness on the pressure is also studied herein. The static pressure contours and local static pressure distribution along the cyclone length are presented in Figures 11 and 12. As can be seen, an increase in the roughness leads to a lower pressure drop at the cyclone walls. In other words, the decreased tangential and axial velocities resulted from an increase in the roughness causes the velocity gradients to drop. As a result, it can be expected that the pressure must be reduced, which is supported by the data depicted in Figures 11 and 12.

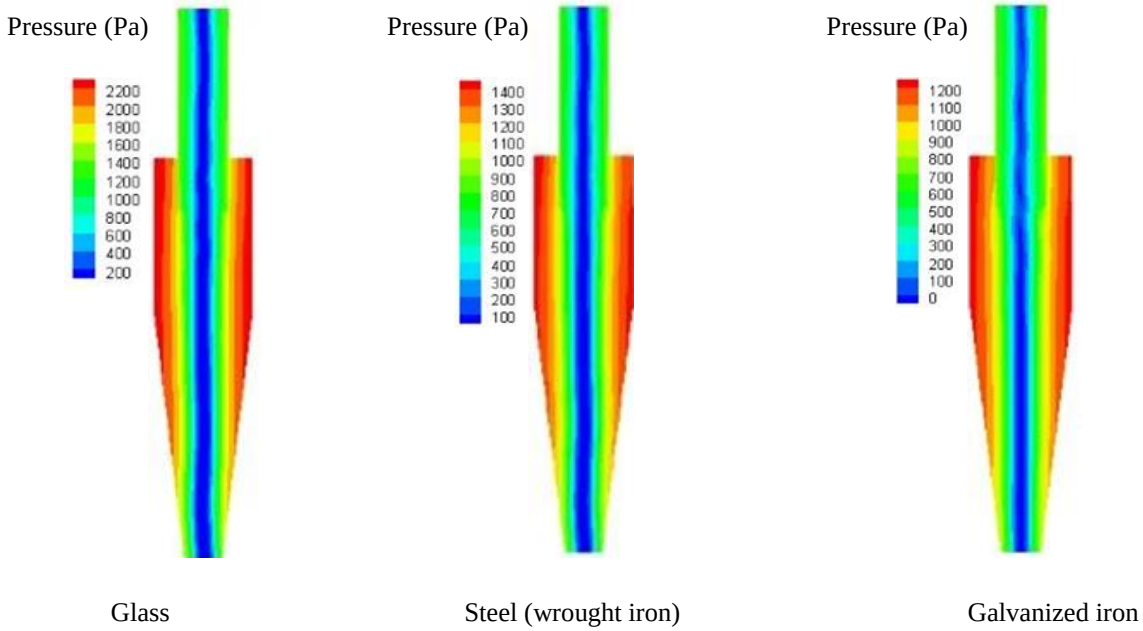

Figure 11

Static pressure at different roughness values.

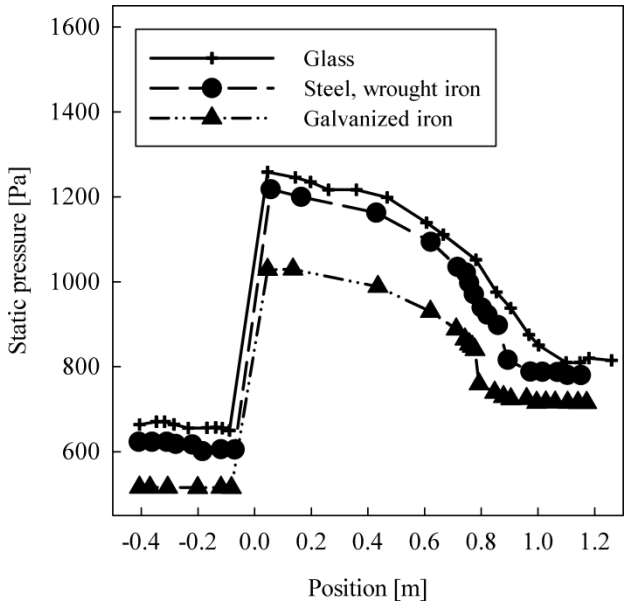

Figure 12

The impact of roughness on static pressure.

The pressure drop is determined as the difference between the static pressure at the inlet and the one at outlet. A higher pressure drop represents higher energy loss during the separation process of droplets. Hence, the decrease of pressure drop is an essential parameter in designing cyclones. According to the results shown in Figure 13a, increasing the roughness and inlet velocity both decrease the pressure drop, so the pressure drop in a cyclone made of glass is much more than that in a cyclone made of galvanized iron.

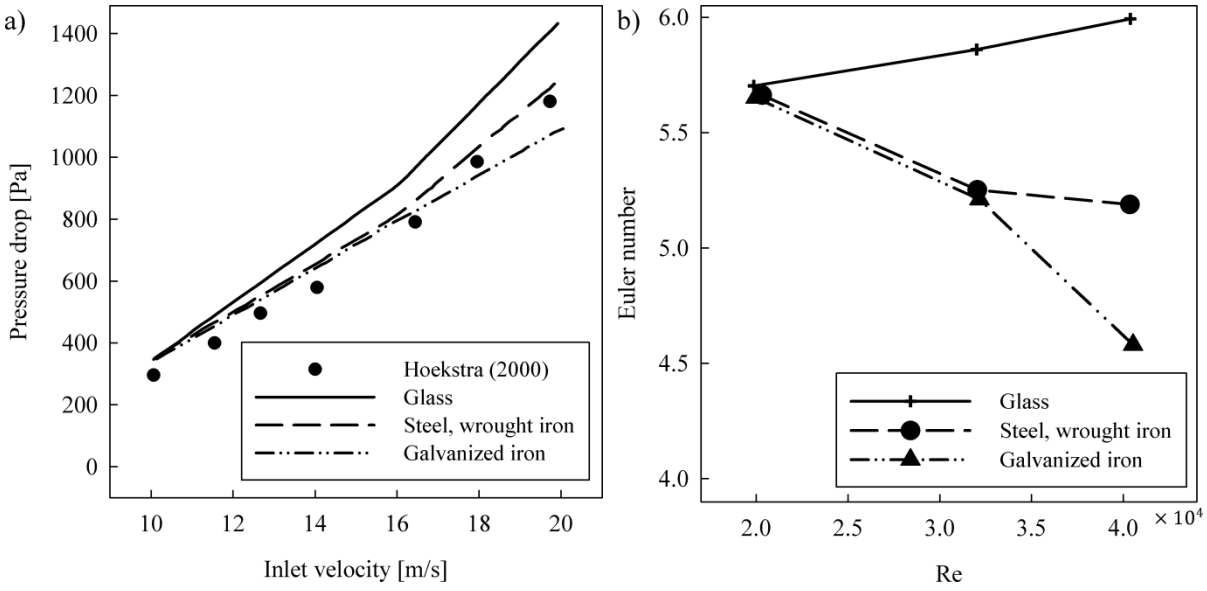

Figure 13

The a) pressure drop and b) pressure drop coefficient (or Euler number) at different roughness values and velocities.

On the other hand, it can be seen that the tangential velocity declines at higher surface roughness. Moreover, the energy loss between the dispersed and continuous phases rises, so the pressure drop increases. The variation in the pressure drop because of changing wall roughness broadens at higher velocities. In this situation, the pressure drop coefficient (or Euler number) is defined as:

$$Eu = \frac{\Delta P}{\frac{1}{2}\rho v_{in}^2} \tag{19}$$

The pressure drop coefficient at various roughness values is delineated in Figure 13b. Increased wall roughness results in decreasing the Euler number at every Reynolds number. Furthermore, it can be inferred from Figure 13b that, for a glass cyclone, an increase in Reynolds number raises Euler number; nonetheless, for a steel (wrought iron) and galvanized iron cyclone, the trend is inverted, that is, an increase in Reynolds number leads to a decrease in pressure drop coefficient.

6.4. Vortex length and the cyclone performance

The vortex length is defined as the axial distance between the outlet tube and the ending vortex flow. It can be seen clearly that the vortex length given in Equations 14 to 16 is defined by three dimensionless geometrical parameters which are not related to the wall roughness. While in the present study, the impact of surface roughness on the vortex length is studied. It can be concluded from Figure 11 that the severe changes in pressure at different wall locations result in a lower vortex length, which affects the cyclone performance from two points of view. It leads to a reduction in

pressure drop, which is preferred; however, it influences the separation efficiency reversely. Figure 14 reveals that vortex length decreases as the surface roughness rises.

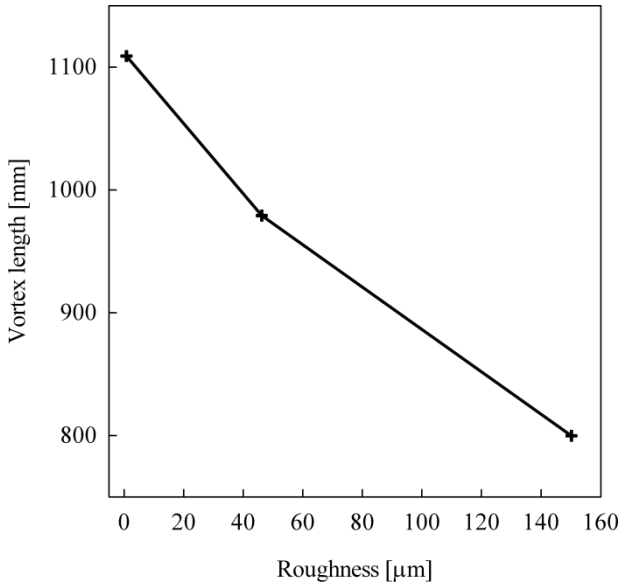

Figure 14

The impact of surface roughness on vortex length.

In fact, the surface roughness leads to friction between gas and the cyclone wall and decreases the gas swirling, which reduces the vortex length and the cyclone efficiency. According to Figure 15, the cyclone separation efficiency improves when it is made of smooth materials like glass rather than rough materials like galvanized steel. Since increasing the surface roughness causes tangential velocity to decline, it may be concluded that increased surface roughness of the cyclone walls results in lower collection efficiency. Nevertheless, the efficiency of the cyclone enhances at higher velocities.

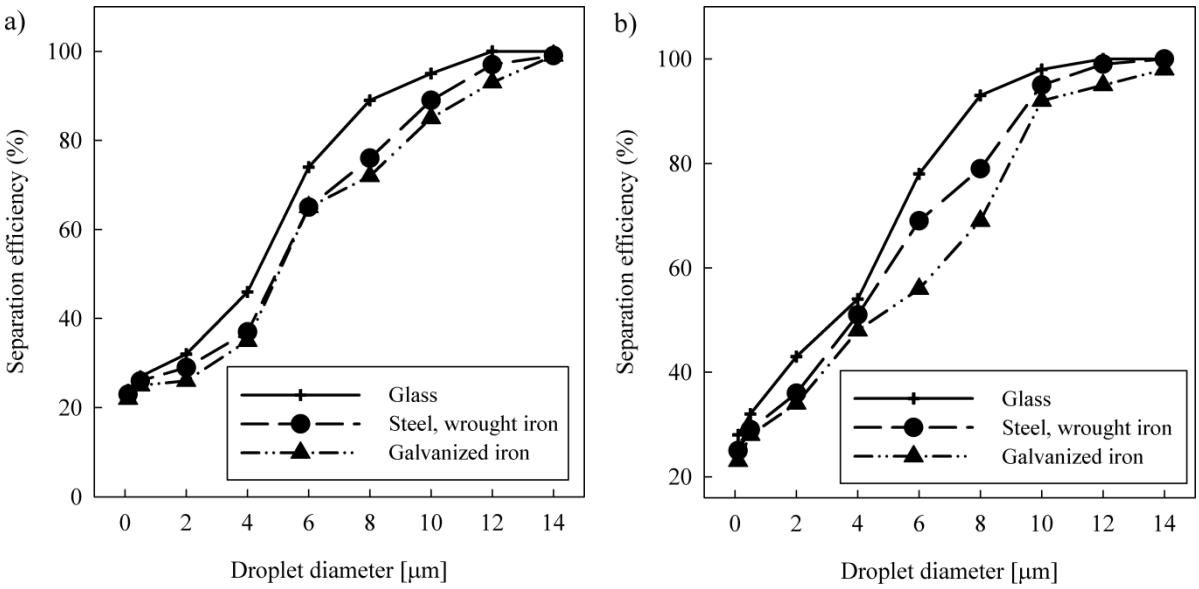

Figure 15

The efficiency of cyclone at different roughness values at a velocity of a) 10 m/s and b) 16 m/s.

7. Conclusions

The wide range of applications of cyclones in industry has inspired many researchers to study the effects of several parameters on the cyclone performance. In the present study, the effects of three values of wall roughness alongside different droplet sizes and various gas inlet velocities on the flow parameters of cyclones are studied. Hence, the radial distribution of axial and tangential velocities and contour plots of pressure distribution are analyzed and presented. Moreover, vortex length and cyclone separation efficiency are investigated numerically. Also, the splashing phenomenon, as a controversial topic among researchers, is considered. The RSM model and Eulerian-Lagrangian approach are employed to simulate the turbulent flow and droplet motion. Finally, based on the results obtained, the following conclusions can be drawn:

- An increase in the surface roughness of the cyclone wall leads to a decline in tangential velocity as the flow resistance rises.
- The surface roughness affects the pressure drop significantly at a higher inlet velocity, while its impact on pressure drop is negligible at lower inlet velocities.
- An increase in the surface roughness of the cyclone wall leads to a decline in swirling flow, the tangential and axial velocities, the pressure drop, and Euler number.
- An increased surface roughness reduces the vortex length and the cyclone efficiency.
- Splashing phenomenon does not happen on the walls of the cyclone.

Nomenclature

C_D	Drag coefficient
F_D	Friction factor (kgm s^{-2})
g	Gravitational acceleration (m s^{-2})
K	turbulence kinetics energy (kgm^2 s^{-2})
$\bar{p}$	Mean pressure (Pa)
P	Stress generation (kgm^{-1} s^{-2})
Q	Volumetric flow rate (m^3 s^{-1})
R_{ij}	Reynolds stress tensor
t_{res}	Droplet resident time (s)
u	x-component of velocity (m s^{-1})
u'	Fluctuating component of velocity (m s^{-1})
$\bar{u}$	Mean velocity (m s^{-1})
v	y-component of velocity (m s^{-1})
$\forall$	Cyclone volume (m^3)
w	z-component of velocity (m s^{-1})
x_i	Location (m)
Greek Symbols	
ν	Kinematic viscosity (m^2 s^{-1})
ν_t	Turbulent viscosity (m^2 s^{-1})
ρ	Density (kg m^{-3})

ε	Turbulence dissipation
μ	Dynamic viscosity (Pa s)
Subscripts	
d	Droplet
t	Turbulence

References

Alahmadi, Y. H., and Nowakowski, A. F., Modified Shear Stress Transport Model with Curvature Correction for the Prediction of Swirling Flow in a Cyclone Separator, Chemical Engineering Science, Vol. 147, p. 150-165, 2016.

Alexander, R. M., Fundamentals of Cyclone Design and Operation, Proceedings of the Australian Institute of Mining Metallurgy, NS, Vol. 152, No. 3, p. 152-153, 1949.

ANSYS Fluent User's Guide, ANSYS Inc., Southpointe, Canonsburg, PA, USA, 2013.

Baltrenas, P., and Chlebnikovas, A., Experimental Research on the Dynamics of Airflow Parameters in a Six-channel Cyclone-separator, Powder Technology, Vol. 643, p. 328–333, 2015.

Barth, W., Berechnung und Auslegung von Zyklonabscheidern Auf Grund Neuerer Untersuchungen, Combustion Heat Power, Vol. 8, No. 1, p. 1-9, 1956.

Brar, L. S., Sharma, R.P., and Elsayed, Kh., The Effect of the Cyclone Length on the Performance of Stairmand High-efficiency Cyclone, Powder Technology, Vol. 286, p. 668-677, 2015.

Bryant, H. S., Silverman, R.W., and Zenz, F. A., How Dust in Gas Affects Cyclone Pressure Drop, Hydrocarbon Process, (United States), Vol. 62, No. 6, 1983.

Ehteram, M. A., Tabrizi, H. B., Mesbah, M., Ahmadi, G., and Mirsalim, M. A., Experimental Study on the Effect of Connecting Ducts on Demisting Cyclone Efficiency, Experimental Thermal and Fluid Science, Vol. 39, p. 26–36, 2012.

Fathizadeh, N., Mohebbi, A., Soltaninejad, S., and Iranmanesh, M., Design and Simulation of High Pressure Cyclones for a Gas City Gate Station Using Semi-empirical Models, Genetic Algorithm and Computational Fluid Dynamics, Journal of Natural Gas Science and Engineering, Vol. 26, p. 313-329, 2015.

Gao, X., Chen, J., Feng, J., and Peng, X., Numerical and Experimental Investigations of the Effects of the Breakup of Oil Droplets on the Performance of Oil–gas Cyclone Separators In Oil-injected Compressor Systems, International Journal of Refrigeration, Vol. 36, No. 7, p. 1894–1904, 2013.

Hoekstra, A. J., Gas Flow Field and Collection Efficiency of Cyclone Separators, PhD Thesis, Delft University of Technology, Netherland, 2000.

Hosseini, S. M., Shahbazi, Kh., and Khosravi Nikou, M. R., A CFD Simulation of the Parameters Affecting the Performance of Downhole Deoiling Hydrocyclone, Iranian Journal of Oil & Gas Science and Technology (IJOGST),Vol. 4, No. 3, p. 77–93, 2015.

Ji, Z. L., Wu, X. L., and Shi, M. X., Experimental Research on the Natural Turning in the Cyclone, Proceedings of Filtech Europa 91 Conference, Vol. 2, p. 583–589, 1991.

Kaya, F., Karagoz, I., and Avci, A., Effects of Surface Roughness on the Performance of Tangential Inlet Cyclone Separators, Aerosol Science and Technology, Vol. 45, No. 8, p. 988-995, 2011.

Karagoz, I., and Avci, A., Modelling of the Pressure Drop in Tangential Inlet Cyclone Separators. Aerosol Science and Technology, Vol. 39, No. 9, p. 857-865, 2005.

Kępa, A., Division of Outlet Flow in a Cyclone Vortex Finder—The CFD Calculations, Separation and Purification Technology, Vol. 75, No. 2, p. 127-131, 2010.

Meißner, P., and Löffler, F., Zur Berechnung des Strömungsfeldes im Zyklonabscheider, Chemical Engineering, Vol. 50, No. 6, p. 471-471, 1978.

Muschelknautz, E., and Krambrock, W., Aerodynamische Beiwerte des Zyklonabscheiders Aufgrund Neuer und Verbesserter Messungen, Chemical Engineering, Vol. 42, No. 5, p. 247-255, 1970.

Sabziani, J., and Sari, A., A CFD Simulation of Hydrogen Production in Microreactors, Iranian Journal of Oil & Gas Science and Technology (IJOGST), Vol. 4, No. 1, p. 35–48, 2015.

Shames, I. H., and Shames, I. H., Mechanics of Fluids, Vol. 2, New York: McGraw-Hill, 1982.

Shi, L., and Bayless, D. J., Comparison of Boundary Conditions for Predicting the Collection Efficiency of Cyclones, Powder Technology, Vol. 173, No. 1, p. 29-37, 2007.

Shukla, S. K., Shukla, P., and Ghosh, P., The Effect of Modeling of Velocity Fluctuations on Prediction of Collection Efficiency of Cyclone Separators, Applied Mathematical Modelling, Vol. 37, No. 8, p. 5774-5789, 2013.

Sun, X., Kim, S., Yang, S. D., Kim, H. S., and Yoon, J. Y., Multi-objective Optimization of a Stairmand Cyclone Separator Using Response Surface Methodology and Computational Fluid Dynamics, Powder Technology, Vol. 320, p. 51-65, 2017.

Parvaz, F., Hosseini, S. H., Ahmadi, G., and Elsayed, Kh., Impacts of the Vortex Finder Eccentricity on the Flow Pattern and Performance of a Gas Cyclone, Separation and Purification Technology, Vol. 187, p. 1-13, 2017.

Raoufi, A., Shams, M., Farzaneh, M., and Ebrahimi, R., Numerical Simulation and Optimization of Fluid Flow in Cyclone Vortex Finder, Chemical Engineering and Processing: Process Intensification, Vol. 47, No. 1, p. 128-137, 2008.

Wang, B., Xu, D. L., Chu, K. W., and Yu, A. B., Numerical Study of Gas–solid Flow in a Cyclone Separator, Applied Mathematical Modelling, Vol. 30, No. 11, p. 1326-1342, 2006.

Xiang, R. B., and Lee, K.W., Exploratory Study on Cyclones of Modified Designs, Particulate Science and Technology, Vol. 19, p. 327–338, 2001.

Zhou, F., Sun, G., Zhang, Y., Ci, H., and Wei, Q., Experimental and CFD Study on the Effects of Surface Roughness on Cyclone Performance, Separation and Purification Technology, Vol. 193, p. 175-183, 2017.